UDC 544.47:546.26-162-31:546.26-169:[542.942.5:547.313.2] doi: 10.33609/2708-129X.92.4.2026.17-28

CATALYTIC PROPERTIES OF CARBON POWDER WITH DEPOSITED REDUCED GRAPHENE OXIDE IN THE ETHYLENE HYDROGENATION.

V.V. Nosach[1,2] http://orcid.org/0000-0003-1278-9507
I.B. Bychko[1] http://orcid.org/0000-0002-4164-3024
P.Ye. Strizhak[1] http://orcid.org/0000-0003-0280-8719

[1]L.V. Pisarzhevskii Institute of Physical Chemistry of National Academy of Sciences of Ukraine, 31 Nauky Avenue, 03028 Kyiv, Ukraine;
[2]National University of "Kyiv-Mohyla Academy", 2 Hryhoriya Skovorody Street, 04655 Kyiv, Ukraine
e-mail: victorynosach@gmail.com

Metal-free catalysts based on carbon powder modified with reduced graphene oxide (rGO) were prepared and investigated in the ethylene hydrogenation reaction. The samples were characterized by Raman and FTIR spectroscopies, SEM, TEM, thermogravimetric analysis, and N_2 adsorption-desorption. SEM and TEM analyses showed that rGO deposition leads to the formation of wrinkled graphene-derived structures covering the external surface of the carbon support. Raman spectra confirmed the presence of defect-rich sp^2-hybridized carbon domains, while FTIR analysis revealed oxygen-containing functional groups associated with partially reduced graphene oxide. Textural analysis demonstrated that rGO incorporation mainly affects the external surface area without significantly changing the microporous structure of the support.

The catalytic properties of the obtained materials were studied in ethylene hydrogenation within 50–400 °C under continuous-flow conditions. The pristine carbon powder provides the highest catalytic activity, whereas deposition of rGO results in a decrease in activity compared with the unmodified support. However, within the rGO/CP series, catalytic activity increased with increasing rGO loading, reaching 18% conversion for rGO(0.1)/CP at 400 °C. At the same time, normalization of the reaction rate to the mass of deposited rGO showed a decrease in specific activity at higher rGO contents, attributed to partial restacking of graphene sheets and blocking of active surface sites.

The obtained results indicate that the catalytic behaviour of the investigated composites is governed by the balance between the intrinsic activity of carbon powder and the contribution of defect-rich graphene-derived domains. The findings highlight the importance of controlling graphene loading and surface accessibility in the design of efficient metal-free carbon catalysts.

Keywords: reduced graphene oxide, carbon powder, ethylene hydrogenation, carbocatalysis.

INTRODUCTION. The catalytic transformation of light hydrocarbons remains a key process in modern chemical technology, where the development of efficient and sustainable catalysts is crucial for energy- and resource-intensive industries. Ethylene, being one of the most important platform molecules in petrochemical production, is widely used in polymer manufacturing, fine organic synthesis, and the fabrication of industrial intermediates. Achieving controlled hydrogenation of alkenes under mild conditions requires catalysts with well-defined active sites and a surface structure capable of selective interaction with unsaturated hydrocarbons [1–3].

Conventional catalytic materials for hydrocarbon hydrogenation are typically highly-dispersed metals on supports such as alumina, silica, or metal oxides, where the role of the support is primarily associated with dispersion, stabilization, and electronic tuning of the active phase [4, 5]. At the same time, the growing demand for sustainable catalytic technologies stimulates the development of alternative catalytic systems based on abundant and environmentally benign materials. However, increasing environmental and economic demands are stimulating the search for metal-free catalytic systems that combine high stability, low cost, and the ability to operate without precious or toxic metals [6]. In this context, carbon-based materials have attracted growing attention due to their structural diversity, thermal stability, and tunable surface functionality [7].

Reduced graphene oxide (rGO) has emerged as a particularly promising component, characterized by a high specific surface area, a defect-rich architecture, and the presence of oxygen-containing functional groups that contribute to adsorption and activation processes [8, 9]. The deposition of rGO onto carbon powders or oxide supports leads to the formation of hybrid interfaces, where wrinkle-like graphene fragments can alter the surface morphology, modify mass-transfer pathways, and change the distribution of active sites [10]. Depending on the rGO loading, such systems may show different catalytic activity, as the balance between accessible defects and excessive graphene coverage can influence the efficiency of hydrocarbon conversion.

Although numerous studies have focused on metal-decorated graphene materials, recent reports indicate that rGO demonstrates catalytic activity in hydrogenation, dehydrogenation, and bond-activation reactions without metallic additives [11–13]. These findings highlight the possibility of designing functional metal-free catalysts based on the structural characteristics of carbon materials, in which surface defects and residual oxygen-containing groups are key factors influencing catalytic performance.

The aim of this work is to determine the influence of reduced graphene oxide content, deposited in controlled amounts onto carbon powder, on the catalytic activity of the resulting composites in ethylene hydrogenation. Structural and morphological characterization of the obtained materials was performed using FTIR and Raman spectroscopies, SEM imaging, and thermogravimetric analysis. The results provide insight into the role of rGO loading on the formation of functional surface regions and reveal correlations between surface modification and catalytic performance in a metal-free carbon-based system.

EXPERIMENT AND DISCUSSION OF THE RESULTS. Samples containing rGO deposited onto carbon powder were prepared by depositing an aqueous suspension of graphene

oxide (GO) with controlled concentrations onto the carbon support. The GO suspension was produced by exfoliation of graphite oxide (GrO), synthesized using a modified Hummers' method followed by ultrasonic treatment [14]. The carbon powder (ABCR) was impregnated with the GO water suspension at a ratio of 1 mL per 1 g of support. After deposition, the materials were dried at 60 °C for 3 h and subsequently thermally reduced in a hydrogen flow at 400 °C for 2 h, yielding reduced graphene oxide (rGO). A series of samples containing 0.0025, 0.01, and 0.1 wt.% rGO was prepared and designated according to rGO loading, rGO(0.0025)/CP, rGO(0.01)/CP, and rGO(0.1)/CP.

The structural and physicochemical properties of the obtained composites were characterized using Raman spectroscopy, Fourier-transform infrared spectroscopy (FTIR), scanning electron microscopy (SEM), transmission electron microscopy (TEM), and thermogravimetric analysis (TGA). Raman spectra were recorded at room temperature using a Raman Senterra confocal dispersive spectrometer (Bruker Optik) equipped with a 532 nm excitation laser operating at a power of 2 mW. FTIR measurements were carried out using a PerkinElmer Spectrum One spectrometer in the range of 400–4000 cm^{-1}. Thermogravimetric analysis was performed on a Discovery SDT 650 thermal analyzer under air and nitrogen atmospheres with a heating rate of 10 °C min^{-1}, enabling the assessment of thermal stability and the determination of carbon content in the samples. The morphology and surface elemental distribution of the composites were investigated by SEM and TEM using MIRA3 TESCAN, Quanta 3D FEG, and JEM-1200EX microscopes. Elemental mapping was conducted by energy-dispersive spectroscopy (EDS) to visualize the spatial distribution of carbon- and oxygen-rich regions associated with the deposited rGO.

The catalytic performance of the samples in ethylene hydrogenation was evaluated under continuous flow conditions with chromatographic monitoring of both the reaction mixture and its products. The analysis was carried out using a custom-built gas chromatograph equipped with a thermal conductivity detector and a Porapak S column. The catalyst was loaded into a fixed-bed tubular reactor between two layers of purified quartz, which were placed above and below the catalyst bed. Hydrogenation of ethylene was performed within the temperature range of 50–400 °C using a feed composed of 10% C_2H_4 and 90% H_2 at a total flow rate of 20 mL/min. The mass of catalyst used in each experiment was 0.2–0.7 g.

The rate of hydrogenation product formation was calculated according to equation (1):

$$r_c = \frac{F_{in} - F_{out}}{m_c}$$

where F_{in} is the initial molar flow rate of ethylene (mol s^{-1}); F_{out} is the molar flow rate of ethylene after reactor (mol s^{-1}); m_c is the mass of the catalyst sample, g.

Figure 1a-b shows SEM images of the pristine CP and rGO(0.1)/CP. SEM image of the pristine carbon powder reveals compact particles with relatively smooth surfaces and block-like fragments, showing only minor surface irregularities. The material is characterized by a predominantly monolithic morphology with flat facets and a limited degree of microstructural development, indicating a low level of surface texturing and the absence of nanoscale features.

In contrast, the SEM image of the rGO-modified sample displays pronounced morphological alterations. Numerous wrinkled, sheet-like and layered structures characteristic of reduced graphene oxide are clearly observed on the particle surfaces and along their edges.

Figure 1 c-d shows SEM images with carbon distribution maps for CP and rGO(0.1)/CP. The elemental mapping results support the morphological observations and reveal clear changes in the surface chemistry after rGO modification. For the sample containing 0.1 wt.% rGO, the composition was determined to be 85 wt.% carbon and 15 wt.% oxygen. In comparison, the pristine support without rGO deposition contains 87 wt.% carbon and 13 wt.% oxygen. Oxygen-containing regions are predominantly located in the areas where the SEM images show film-like and layered structures, which is consistent with the presence of graphene-derived fragments on the surface of the support. The increased oxygen content compared to the pristine material indicates the retention of functional groups within the rGO phase and their contribution to the formation of the surface modification.

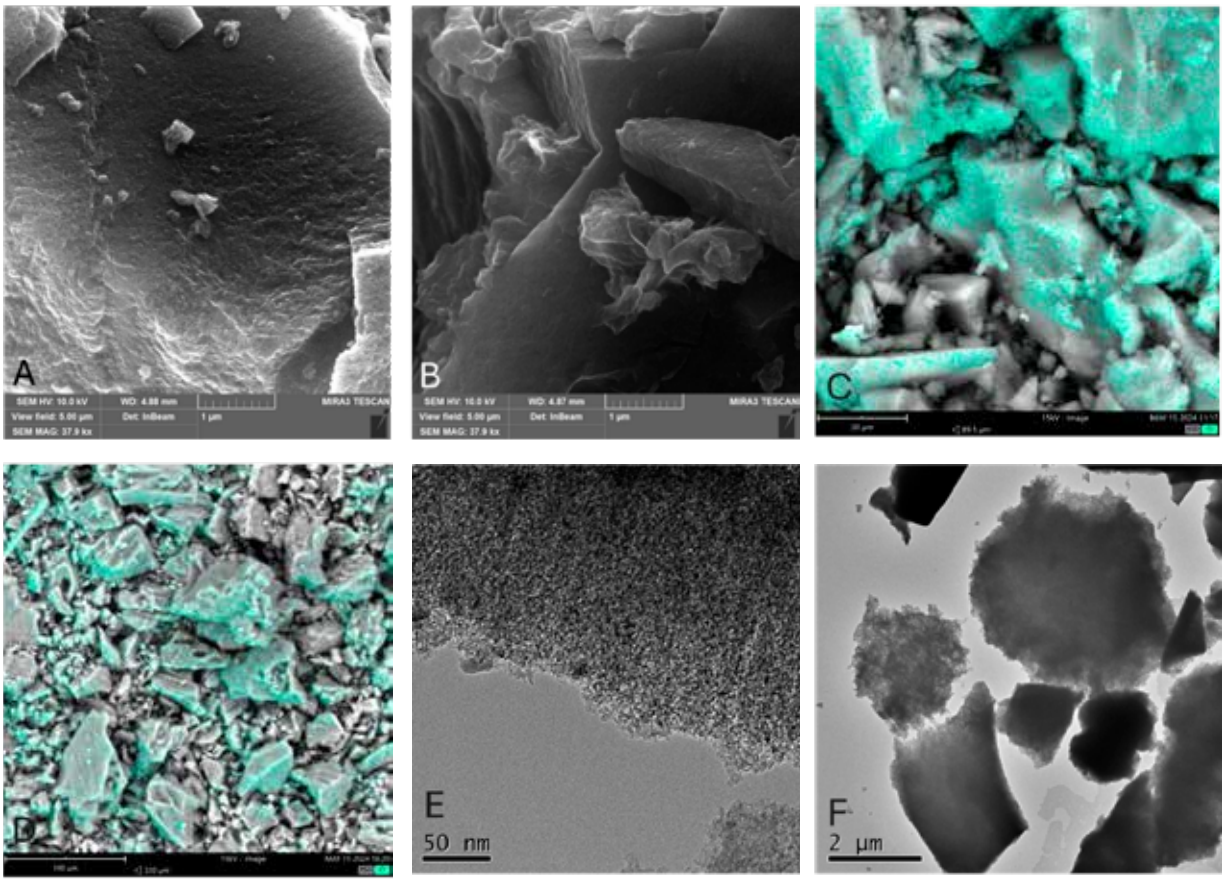

Fig. 1. SEM images of the samples: (a) CP; (b) rGO(0.1)/CP; SEM images with carbon distribution maps on the surfaces of: (c) CP; (d) rGO(0.1)/CP; (e) HRTEM image of CP; (f) TEM image of CP.

Figure 1e–f shows HRTEM and TEM images of the carbon powder (CP). The HRTEM analysis Fig. 1e reveals a disordered carbon structure composed of densely packed nanoscale domains. No clear lattice fringes corresponding to crystalline graphitic planes are observed, indicating a predominantly amorphous or poorly ordered turbostratic structure. The material is characterized by a developed surface with nanoscale heterogeneities. The TEM images Fig. 1f show irregularly shaped particles with a broad size distribution, forming agglomerates up to several micrometres in size. The particles have non-uniform morphology with diffuse boundaries and no well-defined geometric shape, indicating a fragmented structure. TEM analysis was also performed for rGO-modified samples; however, no distinct graphene-derived structures could be reliably identified due to the low rGO loading and insufficient contrast between rGO and the carbon powder surface

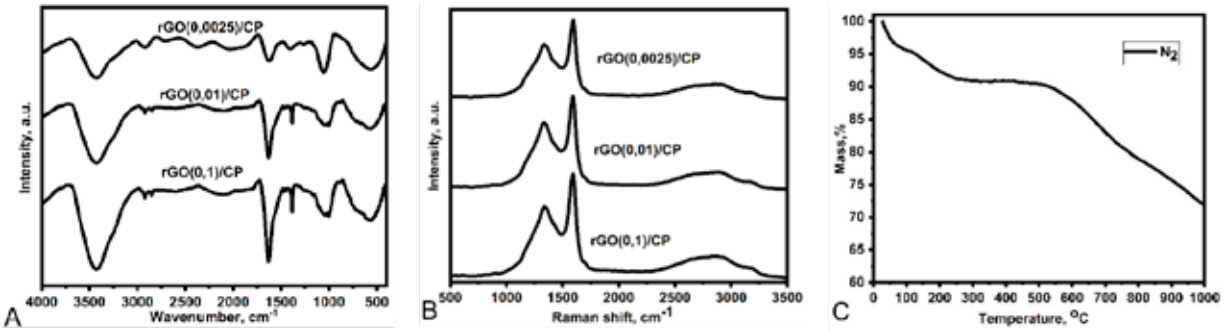

Fig. 2. FTIR (a) and Raman (b) spectra of rGO (0.0025)/CP, rGO (0.01)/CP, rGO (0.1)/CP; (c) thermogram of rGO(0.1)/CP in nitrogen atmosphere.

Figure 2a presents the FTIR spectra of carbon powder samples modified with different loadings of reduced graphene oxide. All spectra show weak-to-moderate absorption features typical of carbon-based materials containing residual oxygen functionalities. A broad band near 3400 cm^{-1} is commonly associated with O–H stretching vibrations of hydroxyl groups and adsorbed moisture [23]. Weak bands in the 2850–2950 cm^{-1} region can be assigned to C–H stretching vibrations originating from aliphatic fragments or residual organic species [24]. A distinct band at approximately 1700–1720 cm^{-1} is generally attributed to C=O stretching of carbonyl and carboxyl groups, while the absorption close to ~1600 cm^{-1} is usually linked to C=C stretching within sp^2-hybridised carbon structures [25]. Bands appearing in the 1400–1200 cm^{-1} region are commonly associated with C–OH and C–O vibrations, and signals in the ~1100–1000 cm^{-1} range are indicative of C–O–C stretching modes related to epoxide and ether functionalities that may remain in partially reduced graphene oxide [26]. The band observed near ~2350 cm^{-1} can be attributed to atmospheric CO_2 [27]. Comparison of the spectra suggests that oxygen-related bands become slightly more pronounced with increasing rGO content, indicating progressive enrichment of the surface with rGO-derived functional groups.

Figure 2b shows the Raman spectra of carbon powder samples modified with different loadings of reduced graphene oxide. All rGO-containing samples have two characteristic bands of sp^2-hybridised carbon materials: the D band at 1350 cm^{-1}, associated with disorder-induced scattering, and the G band in the 1580–1600 cm^{-1} region, corresponding to the in-plane vibration of graphitic carbon atoms. With increasing rGO content, the D band becomes more pronounced relative to the G band, indicating an increase in the defect density and structural disorder within the carbon framework [28]. In addition to the main D and G bands, a weak D′ band is observed at around 1620–1630 cm^{-1}, which is commonly associated with defect-related modes in graphitic structures. A broad 2D band is observed at 2680–2720 cm^{-1} and remains of low intensity, with only a minor enhancement at higher rGO loadings [29]. Overall, the evolution of the Raman spectra suggests that incorporation of rGO increases the degree of structural disorder in the carbon powder, consistent with the introduction of defect-rich graphene-derived domains.

Figure 2c shows the thermogravimetric behaviour of the carbon powder/rGO sample in an inert nitrogen atmosphere, demonstrating a stepwise mass loss typical for carbon-based materials. At temperatures up to 120 °C, the sample loses 5% of its mass, mainly due to the desorption of physically adsorbed moisture and residual volatiles. Further heating to 300 °C results in an additional mass loss of 4%, which can be attributed to the thermal decomposition of oxygen-containing surface functional groups associated with rGO and the carbon support. In the 300–500 °C range, the mass change remains minimal (~0.48%), indicating relatively high thermal stability of the carbon framework. At higher temperatures, the mass loss becomes more pronounced, reaching 11% between 500 and 800 °C and a further 7% between 800 and 1000 °C. The total mass loss of approximately 28% at 1000 °C confirms that a substantial fraction of the carbon framework remains intact under non-oxidising conditions.

Table 1.

Textural characteristics of CP and rGO/CP samples.

	Specific surface area, S, $m^2\ g^{-1}$	Total pore volume, V_p, $cm^3\ g^{-1}$	Micropore volume, V_m, $cm^3\ g^{-1}$	t-Plot External Surface Area, $m^2\ g^{-1}$
CP	1880	1.46	0.62	150
rGO (0.0025)/CP	1930	1.45	0.62	620
rGO (0.01)/CP	1720	1.46	0.62	670
rGO (0.1)/CP	1920	1.48	0.62	690

The textural parameters of the CP and rGO-modified CP samples are summarized in Table 1. The pristine CP exhibits a specific surface area of 1880 $m^2\ g^{-1}$, a total pore volume of 1.46 $cm^3\ g^{-1}$, and a micropore volume of 0.62 $cm^3\ g^{-1}$. The incorporation of rGO leads to slight variations in the specific surface area depending on its loading. The highest value among the modified samples is observed for rGO(0.0025)/CP (1930 $m^2\ g^{-1}$), while a more

pronounced decrease to 1720 $m^2 g^{-1}$ occurs at the intermediate loading (rGO(0.01)/CP), followed by an increase to 1920 $m^2 g^{-1}$ for rGO(0.1)/CP. A similar trend is observed for the total pore volume, which remains in the range of 1.45–1.48 $cm^3 g^{-1}$ for all samples. In contrast, the micropore volume remains constant at 0.62 $cm^3 g^{-1}$ for both pristine and rGO-modified materials, indicating that the introduction of rGO does not significantly alter the microporous fraction. The substantial increase in observed t-plot external surface area from 150 $m^2 g^{-1}$ for CP to 620-690 $m^2 g^{-1}$ for rGO-deposited samples is a consequence of several effects. Mainly, a contribution of additional surface area, formation of carbon–rGO gaps, and increased surface roughness and fractality due to the introduction of additional corrugation and defects, increasing the geometric complexity of the outer surface as a consequence of rGO deposition.

These results suggest that rGO incorporation mainly affects the external surface and mesoporous structure rather than generating additional microporosity. Overall, rGO modification does not lead to a substantial increase in surface area compared to pristine CP, but significantly increases surface area, which is not associated with micropores.

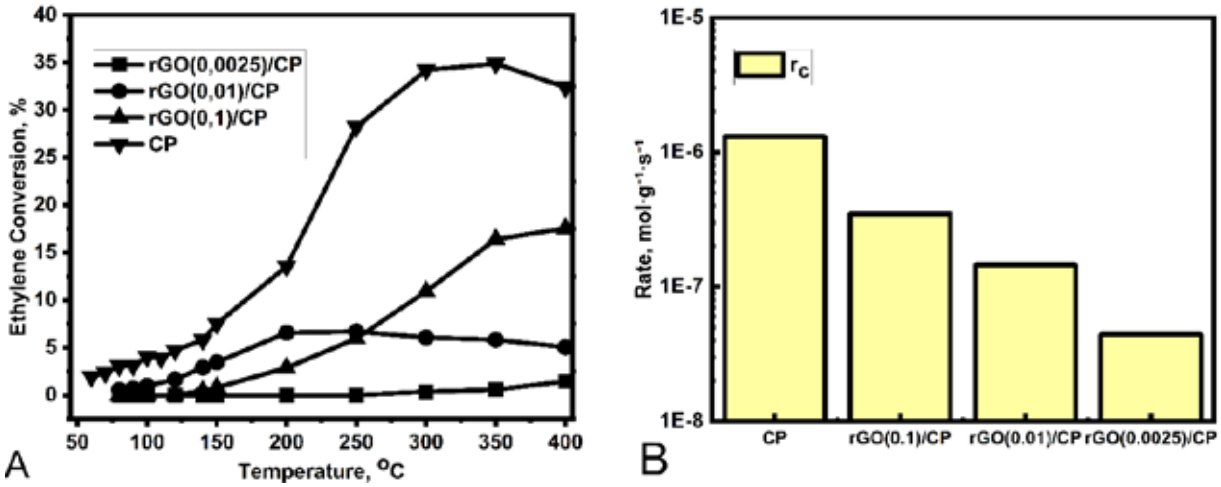

Fig. 3. (a) Temperature dependence of ethylene conversion in the process of ethylene hydrogenation within the temperature range of 50-400 °C, total flow rate 20 mL/min; Conversion of ethylene for ■ – rGO(0.0025)/CP; ● – rGO(0.01)/CP; ▲ – rGO(0.1)/CP; ▼ – CP. (b) Reaction rate diagrams of ethylene hydrogenation over CP, rGO (0.0025)/CP, rGO (0.01)/CP, rGO (0.1)/CP, recalculated per catalyst mass at 400°C. r_c – rate of ethylene hydrogenation normalized to the mass of the catalyst.

Figure 3a shows the temperature dependence of ethylene conversion over pristine carbon powder (CP) and rGO-modified CP catalysts. For the CP sample, conversion starts at 2% at 60 °C and gradually increases to 14% at 200 °C. Upon further heating, a sharp rise is observed, with conversion reaching 28% at 250 °C and exceeding 30% at temperatures above 300 °C.

The maximum conversion of 35% is achieved at 350 °C, followed by a slight decrease to 32% at 400 °C. For the rGO(0.0025)/CP catalyst, ethylene conversion remains below 1% over the investigated temperature range, reaching a maximum of 1% at 400 °C. The rGO(0.01)/CP catalyst becomes active already at 80 °C, providing an ethylene conversion of 1%, and shows a continuous increase in the low- and intermediate-temperature region. The conversion reaches 3% at 150 °C and attains its maximum value of 7% at 250 °C. At higher temperatures, a gradual decrease is observed, with conversion declining to 6% at 300 °C, 6% at 350 °C, and 5% at 400 °C. In contrast, the rGO(0.1)/CP catalyst remains inactive up to 140 °C. With increasing temperature, the conversion rises progressively to 3% at 200 °C and 6% at 250 °C, followed by a more pronounced increase in the high-temperature region. The conversion reaches 11% at 300 °C and increases further to 16% at 350 °C, achieving a maximum of 18% at 400 °C.

Figure 3b shows the reaction rate values for ethylene hydrogenation at 400 °C over carbon powder (CP) and rGO/CP catalysts. The pristine carbon powder has the highest activity, with a reaction rate of $1.3 \cdot 10^{-6}$ mol·g(cat)$^{-1}$·s^{-1}. Deposition of rGO decreases the reaction rate compared to pristine CP. The sample containing 0.0025 wt.% rGO has a reaction rate of ethylene hydrogenation $4.4 \cdot 10^{-8}$ mol·g(cat)$^{-1}$·s^{-1}, which increases to $1.4 \cdot 10^{-7}$ mol·g(cat)$^{-1}$·s^{-1} for 0.01 wt.% rGO, and reaches $3.5 \cdot 10^{-7}$ mol·g(cat)$^{-1}$·s^{-1} for the catalyst with 0.1 wt.% rGO. These results indicate that although rGO incorporation does not outperform the pristine carbon powder under the studied conditions, higher rGO loading partially improves the activity within the composite catalyst series. Overall, the obtained data demonstrate that the catalytic behaviour of the carbon/rGO composites strongly depends on rGO loading. While pristine CP remains the most active material at 400 °C, the reaction rate within the rGO-modified series increased progressively with increasing rGO content.

The obtained results demonstrate that the catalytic behaviour of the investigated materials in ethylene hydrogenation is governed primarily by the activity of the CP. SEM analysis reveals that rGO forms wrinkled, sheet-like, and layered domains covering the surface of the carbon particles, which is consistent with t-plot analysis. Such coverage leads to partial blocking of the outer surface of carbon support, whereas the main surface of CP is localized in the micropores. Therefore, it can be proposed that active sites on the surface of CP are localized on the outer surface of CP particles, whereas the surface of CP that is localized in the micropores contains a minor fraction of active sites. Analysis shows that since the micropore volume remains essentially constant for all samples, diffusion limitations associated with high microporosity can be excluded for the observed catalytic behavior. This indicates that, for the studied reaction, the overall surface area is not the determining factor, and the reaction rate is governed by a combination of factors.

The catalytic activity of graphene-derived carbon materials in hydrogenation reactions, and particularly in ethylene hydrogenation, was demonstrated previously [30]. Whereas the detailed mechanism remains undefined, the surface structural defects, such as vacancy-type defects, are considered as adsorption sites for hydroden dissociative adsorption, and ethylene is proposed to be activated by a π-π

stacking. This means that in the rGO/CP system, there are two catalytically active phases, the CP and rGO. Whereas deposition of rGO on CP results in the decrease of catalytic activity of CP due to the blocking of active sites, the increase of the ethylene hydrogenation rate with the increase of rGO content shows that rGO remains catalytically active after its deposition on CP. An increase of rGO content by 4 times, from 0.0025 wt.% to 0.01 wt.%, leads to an increase in the ethylene hydrogenation rate by 3.2 times. This indicates that deposited rGO in very small amounts does not restack and allows for the approximation of a rate of ethylene hydrogenation associated with rGO. The obtained rate is $1.3{\cdot}10^{-}5$ mol·g(rGO)$^{-1}$·s^{-1}, which is consistent with the ethylene hydrogenation rate on rGO reported previously in such conditions [30]. Deposition of higher amounts of rGO by 10 times, from 0.01 wt.% to 0.1 wt.%, leads to an unproportional increase in ethylene hydrogenation rate by 2.5 times, which can be caused by a significant restacking of rGO sheets during its deposition in this concentration range.

Therefore, the catalytic performance of the investigated metal-free carbon-based systems is non-additive and determined by a combination of the active sites of the carbon powder and introducing additional defect-rich rGO through surface modification. In the present composites, rGO deposition predominantly leads to partial deactivation of an intrinsically active carbon support due to site blocking.

CONCLUSIONS. Therefore, the results indicate that the strategy of enhancing catalytic performance through deposition of active rGO onto an activated carbon support may not always lead to the expected synergistic effect, due to the non-additive behavior of the system components. The pristine carbon powder exhibited the highest catalytic activity, achieving an ethylene conversion of 32% and a reaction rate of $1.3{\cdot}10^{-6}$ mol·g(cat)$^{-1}$·s^{-1} at 400 °C. Within the rGO/CP series, the catalytic activity increased with increasing rGO loading, reaching a maximum conversion of 18% for the rGO(0.1)/CP sample. At the same time, normalization of the reaction rate to the mass of deposited rGO showed a decrease in specific activity at higher rGO loadings, which was attributed to partial restacking of rGO sheets and blocking of active surface sites. These findings highlight the sensitivity of surface-active sites and suggest that partial coverage of the outer surface plays a key role.

Importantly, these observations open up clear directions for improved catalyst design. Future efforts can focus on the deliberate introduction of chemically distinct active sites or on optimizing graphene-derived materials in combination with suitable supports, where surface modification promotes the formation of new reactive centers rather than limiting access to existing ones. This approach offers a promising pathway toward achieving enhanced catalytic performance through more targeted material engineering.

AUTHOR CONTRIBUTIONS:

V. V. Nosach: investigation, methodology, data curation, formal analysis, visualization, writing – original draft.

I. B. Bychko: conceptualization, methodology, writing – review & editing.

P. Ye. Strizhak: conceptualization, supervision, writing – review & editing, funding acquisition.

All authors have read the results of the study and approved the final version of the manuscript.

CONFLICT OF INTEREST. The authors declare no conflict of interest.

FUNDING. This work was carried out with financial support from a grant provided by the Simons Foundation (ID: SFI-PD-Ukraine-00014577 (2025)).

ACKNOWLEDGMENTS. Raman spectroscopy, thermogravimetric analysis (TGA), and scanning electron microscopy with elemental mapping (SEM–EDS) were performed at Nicolaus Copernicus University. The authors would like to thank Prof. Wojciech Kujawski, PhD, DSc, for his support.

КАТАЛІТИЧНІ ВЛАСТИВОСТІ ВІДНОВЛЕНОГО ОКСИДУ ГРАФЕНУ, НАНЕСЕНОГО НА ВУГЛЕЦЕВИЙ ПОРОШОК, У РЕАКЦІЇ ГІДРУВАННЯ ЕТИЛЕНУ

В. В. Носач[1,2], І. Б. Бичко[1], П. Є. Стрижак[1]

[1]Інститут фізичної хімії ім. Л. В. Писаржевського Національної академії наук України, просп. Науки, 31, Київ, 03028, Україна;
[2]Національний університет «Києво-Могилянська академія», вул. Григорія Сковороди, 2, Київ 04655, Україна
e-mail: victorynosach@gmail.com

Неметалеві каталізатори на основі вуглецевого порошку з нанесеним відновленим оксидом графену (rGO) з різним вмістом було синтезовано та досліджено в реакції гідрування етилену. Отримані зразки охарактеризовано методами раманівської та ІЧ-Фур'є-спектроскопії (FTIR), скануальної електронної мікроскопії (SEM), трансмісійної електронної мікроскопії (TEM) і термогравіметричного аналізу. Вихідний вуглецевий порошок продемонстрував найвищу каталітичну активність, тоді як нанесення rGO призводить до зниження ступеня перетворення етилену та швидкості реакції порівняно з немодифікованим носієм. Водночас у серії rGO/CP активність зростає зі збільшенням вмісту rGO, причому найвищі показники спостерігаємо для зразка з 0,1 мас.% rGO. Швидкості реакції у перерахунку на масу нанесеного rGO показали зменшення каталітичної активності зі зростанням його вмісту. Припускаємо, що нанесення rGO на активний вуглецевий носій може призводити до часткового блокування активних центрів.

Ключові слова: відновлений оксид графену, вуглецевий порошок, гідрування етилену, карбокаталіз.

REFERENCES

1. Zhang J., Su D. S., Zhang A., Wang D., Schlögl R., Hébert C. Nanocarbon as Robust Catalyst: Mechanistic Insight into Carbon-Mediated Catalysis. Angew Chem Int Ed. 2007. **46**: 7319–7323. https://doi.org/10.1002/anie.200702466
2. Radovic L. R., Bockrath B. On the chemical nature of graphene edges: Origin of stability and reactivity. J Am Chem Soc. 2005. **127**(16): 5917–5927. https://doi.org/10.1021/ja050124h
3. Serp P., Machado B. Nanostructured Carbon Materials for Catalysis. Cambridge: RSC Publishing. 2015. https://doi.org/10.1039/9781782622567

4. Pan X., Bao X. The effects of confinement inside carbon nanotubes on catalysis. Acc Chem Res. 2011. **44**(8): 553–562. https://doi.org/10.1021/ar100160t
5. Wang X., Li W., Chen Z., Waje M., Yan Y. Durability investigation of carbon nanotube as catalyst support for proton exchange membrane fuel cell. J Power Sources. 2006. **158**: 154–159. https://doi.org/10.1016/j.jpowsour.2005.09.039
6. Liu X., Dai L. Carbon-based metal-free catalysts. Nat Rev Mater. 2016. **1**: 16064. https://doi.org/10.1038/natrevmats.2016.64
7. Su D. S., Wen G., Wu S., Peng F., Schlögl R. Carbocatalysis in liquid-phase reactions. Angew Chem Int Ed. 2017. **56**: 936–964. https://doi.org/10.1002/anie.201600906
8. Dreyer D. R., Park S., Bielawski C. W., Ruoff R. S. The chemistry of graphene oxide. Chem Soc Rev. 2010. **39**: 228–240. https://doi.org/10.1039/B917103G
9. Kim J., Cote L. J., Kim F., Huang J. Revealing the Nature of Interaction between Graphene Oxide and Lipid Membrane by Surface-Enhanced Infrared Absorption Spectroscopy. J Am Chem Soc. 2015. **137**(32): 10052–10055. https://doi.org/10.1021/jacs.5b03803
10. Dong L., Gari R. R. S., Li Z., Craig M. M., Hou S. Graphene-supported metal nanoparticles for heterogeneous catalysis. Carbon. 2010. **48**: 781–787. https://doi.org/10.1016/j.carbon.2009.10.027
11. Qu L., Liu Y., Baek J-B., Dai L Nitrogen-doped graphene as efficient metal-free electrocatalyst for oxygen reduction. ACS Nano. 2010. **4**(3): 1321–1326. https://doi.org/10.1021/nn901850u
12. Tang Y., Allen B. L, Kauffman D. R., Star A. Electrocatalytic activity of nitrogen-doped carbon nanotube cups. J Am Chem Soc. 2009. **131**(37): 13200–13201. https://doi.org/10.1021/ja9055408
13. Wang H., Maiyalagan T., Wang X. Review on recent progress in nitrogen-doped graphene: Synthesis, characterization, and its potential applications. ACS Catal. 2012. **2**(5): 781–794. https://doi.org/10.1021/cs200652y
14. Nosach V. V., Bychko I. B., Strizhak P. E. Catalytic properties of reduced graphene oxide deposited on aluminium oxide in the process of ethane dehydrogenation. Theor Exp Chem. 2025. **61**: 141–147. https://doi.org/10.1007/s11237-025-09860-w
15. Sádovská G., Martincic M., Vacik J., et al. The thermal stability of carbon materials in the air: Quantitative structural investigation of thermal stability of carbon materials in air. Carbon. 2023. **205**: 110–121. https://doi.org/10.1016/j.carbon.2023.02.042
16. Khasraw D., Spooner S., Hage H., et al. Evaluation of devolatilization behaviour of different carbonaceous materials under rapid heating for the novel HIsarna ironmaking process. Fuel. 2021. **292**: 120329. https://doi.org/10.1016/j.fuel.2021.120329
17. Suter J. L, Sinclair R. C., Coveney P. V. Principles governing control of aggregation and dispersion of graphene and graphene oxide in polymer melts. Adv Mater. 2020. **32**(36): 2003213. https://doi.org/10.1002/adma.202003213
18. Rissanou A., Karnis I., Krasanakis F., et al. The role of oxidation pattern and water content in the spatial arrangement and dynamics of oxidized graphene-based aqueous dispersions. Int J Mol Sci. 2022. **23**(21): 13459. https://doi.org/10.3390/ijms232113459
19. Mases M., Palmqvist A. E. C., Gustafson J. The oxidation of carbon nanostructures imaged by electron microscopy: Comparison between in-situ TEM and TGA experiments. Appl Surf Sci. 2024. **663**: 160755. https://doi.org/10.1016/j.apsusc.2024.160755
20. Panerai F., Martin A., De Porte J. M., et al. Flow-tube oxidation experiments on the carbon preform of a phenolic-impregnated carbon ablator. J Thermophys Heat Transfer. 2014. **28**(2): 181–190. https://doi.org/10.2514/1.T4265

21. Li W., Liu X., Chen Y., et al. The fate of aggregated graphene oxide upon the increasing of pH: An experimental and molecular dynamic study. Sci Total Environ. 2022. **824**: 153855. https://doi.org/10.1016/j.scitotenv.2022.157954
22. Martincic M., Sádovská G., Vacik J., et al. Thermal stability and purity of graphene and carbon nanotubes: Key parameters for their thermogravimetric analysis (TGA). Nanomaterials. 2024. **14**(21): 1754. https://doi.org/10.3390/nano14211754
23. He H., Klinowski J., Forster M., Lerf A. A new structural model for graphite oxide. Chem Phys Lett. 1998. **287**: 53–56. https://doi.org/10.1016/S0009-2614(98)00144-4
24. Stankovich S., Dikin D. A., Dommett G. H. B., et al. Graphene-based composite materials. Nature. 2006. **442**: 282–286. https://doi.org/10.1038/nature04969
25. López P., Gómez-Romero P., González A., Martín C. Surface characteristics and electrochemical behavior of partially reduced graphene oxide. Electrochim Acta. 2013. **106**: 556–563. https://doi.org/10.1016/j.electacta.2017.06.071
26. Eda G., Chhowalla M. Chemically derived graphene oxide: Towards large-area thin-film electronics and optoelectronics. Adv Mater. 2010. **22**: 2392–2415. https://doi.org/10.1002/adma.200903689
27. Stuart B. Infrared Spectroscopy: Fundamentals and Applications. Chichester: John Wiley & Sons. 2004.
28. Rodríguez-Reinoso F. The role of carbon materials in heterogeneous catalysis. Carbon. 1998. **36**: 159–175. https://doi.org/10.1016/S0008-6223(97)00173-5
29. Ferrari A. C., Robertson J. Interpretation of Raman spectra of disordered and amorphous carbon. Phys Rev B. 2000. **61**: 14095–14107. https://doi.org/10.1103/PhysRevB.61.14095
30. Perhun T. I., Bychko I. B., Trypolsky A. I., et al. Catalytic properties of graphene material in the hydrogenation of ethylene. Theor Exp Chem. 2013. **48**: 367–370. https://doi.org/10.1007/s11237-013-9282-1

Стаття надійшла: 28.03.2026.
Статтю прийнято до друку: 10.05.2026.
Статтю опубліковано: 25.05.2026.